Experimental classification of entanglement in arbitrary three-qubit pure states on an NMR quantum information processor

Amandeep Singh,[*] Harpreet Singh,[†] Kavita Dorai,[‡] and Arvind[§]
Department of Physical Sciences, Indian Institute of Science Education & Research Mohali, Sector 81 SAS Nagar, Manauli PO 140306, Punjab, India

(Received 7 May 2018; published 4 September 2018)

We undertake experimental detection of the entanglement present in arbitrary three-qubit pure quantum states on an NMR quantum information processor. Measurements of only four observables suffice to experimentally differentiate between the six classes of states which are inequivalent under stochastic local operation and classical communication. The experimental realization is achieved by mapping the desired observables onto Pauli z operators of a single qubit, which is directly amenable to measurement. The detection scheme is applied to known entangled states as well as to states randomly generated using a generic scheme that can construct all possible three-qubit states. The results are substantiated via direct full quantum state tomography as well as via negativity calculations and the comparison suggests that the protocol is indeed successful in detecting tripartite entanglement without requiring any *a priori* information about the states.

DOI: 10.1103/PhysRevA.98.032301

I. INTRODUCTION

Quantum entanglement plays a fundamental role in quantum information processing and is a key resource for several quantum computational and quantum communication tasks [1]. Any experiment aimed at entanglement generation needs as an integral part a way to establish that entanglement has indeed been generated [2]. Therefore, the detection of entanglement and its characterization is a foundational problem and is a key focus of research in quantum information processing [3]. Entanglement detection and certification protocols include quantum state tomography [4], entanglement witness operators [5–7] of the density operator under partial transposition [8,9], and the violation of Bell's inequalities [10].

Experimentally, entanglement has been created in various physical systems including nitrogen-vacancy defect centers [11], trapped-ion quantum computers [12], superconducting phase qubits [13], nuclear-spin qubits [14], and quantum dots [15]. Bound entanglement was created and detected by using three nuclear spins [16] and there have been several efforts to create and detect three-qubit entanglement by using NMR [17–21]. Witness-based entanglement detection protocols have been implemented experimentally in quantum optics [22] and NMR [23]. Concurrence [24] was measured by a single measurement on twin copies of the quantum state of photons [25] while entanglement of formation was used as an entanglement quantifier in four trapped ions [26]. Although there has been various experimental advances to detect entanglement, characterizing entanglement experimentally as well as computationally remains a daunting task [27–30]. Therefore it is desirable to invent and implement protocols to certify the existence of entanglement which are not intensive on resources.

In the present study we undertake the experimental characterization of arbitrary three-qubit pure states. The three-qubit states can be classified into six inequivalent classes [31] under stochastic local operation and classical communication (SLOCC) [32]. Protocols have been invented to carry out the classification of three-qubit states into the SLOCC classes [33,34]. A recent proposal aims to classify any three-qubit pure entangled state into these six inequivalent classes by measuring only four observables [35]. We have previously constructed a scheme to experimentally realize a canonical form for general three-qubit states, which we use here to prepare arbitrary three-qubit states with an unknown amount of entanglement. Experimental implementation of the entanglement detection protocol is such that, in a single shot, we were able to determine if a state belongs to the Greenberger–Horne–Zeilinger (GHZ) class. We use our previously designed scheme to map the desired observables onto the z magnetization of one of the subsystems, making it possible to experimentally measure its expectation value on NMR systems [36]. Mapping of the observables onto Pauli z operators of a single qubit facilitates the experimental determination of the desired expectation value, since the NMR signal is proportional to the ensemble average of the Pauli z operator.

We implement the protocol on known three-qubit entangled states such as the GHZ state and the W state and also implement it on randomly generated arbitrary three-qubit states with an unknown amount of entanglement. Seven representative states belonging to the six SLOCC inequivalent classes as well as twenty random states were prepared experimentally, with state fidelities ranging between 89% to 99%. To decide the entanglement class of a state, the expectation values of four observables were experimentally measured in the state under investigation. All seven representative states (namely,

[*]amandeepsingh@iisermohali.ac.in
[†]harpreetsingh@iisermohali.ac.in
[‡]kavita@iisermohali.ac.in
[§]arvind@quantumphys.org

GHZ, W, $W\overline{W}$, three biseparable states, and a separable state) were successfully detected within the experimental error limits. By using this protocol, the experimentally randomly generated arbitrary three-qubit states were correctly identified as belonging to either the GHZ, the W, the biseparable, or the separable class of states. We also perform full quantum state tomography to directly compute the observable value. Reconstructed density matrices were used to calculate the entanglement by computing negativity in each case, and the results compared well with those of the current protocol.

This paper is organized as follows: Section II briefly describes the theoretical framework, while the mapping of the required observables onto single-qubit z magnetization is discussed in Sec. II. Section III presents the experimental implementation of the entanglement characterization protocol on a three-qubit NMR quantum information processor. Section IV contains some concluding remarks.

II. DETECTING TRIPARTITE ENTANGLEMENT

There are six SLOCC inequivalent classes of entanglement in three-qubit systems; namely, the GHZ, W, three different biseparable classes, and the separable class [31]. A widely used measure of entanglement is the n-tangle [37,38] and a nonvanishing three-tangle is a signature of the GHZ entangled class and can hence be used for their detection. For three parties A, B, and C, the three-tangle τ is defined as

$$\tau = C^2_{\mathrm{A(BC)}} - C^2_{\mathrm{AB}} - C^2_{\mathrm{AC}}, \tag{1}$$

with C_{AB} and C_{AC} being the concurrence that characterizes entanglement between A and B and between A and C, respectively; $C_{\mathrm{A(BC)}}$ denotes the concurrence between A and the joint state of the subsystem comprising B and C [39].

The idea of using the three-tangle to investigate entanglement in three-qubit generic states is particularly interesting and general, because any three-qubit pure state can be written in the canonical form [40]

$$|\psi\rangle = a_0|000\rangle + a_1 e^{i\theta}|100\rangle + a_2|101\rangle + a_3|110\rangle + a_4|111\rangle, \tag{2}$$

where $a_i \geqslant 0$, $\sum_i a_i^2 = 1$, and $\theta \in [0, \pi]$, and the class of states is written in the computational basis $\{|0\rangle, |1\rangle\}$ of the qubits. The three-tangle for the generic state given in Eq. (2) turns out to be [35]

$$\tau_\psi = 4a_0^2 a_4^2. \tag{3}$$

A three-tangle can be measured experimentally by measuring the expectation value of the operator $O = 2\sigma_x^1\sigma_x^2\sigma_x^3$, in the three-qubit state $|\psi\rangle$. Here, σ_x, σ_y, and σ_z are the Pauli matrices, $i = 1, 2, 3$ denotes the qubit label, and the tensor product symbol between the Pauli operators has been omitted for brevity. Since $\langle\psi|O|\psi\rangle^2 = \langle O\rangle^2_\psi = 4\tau_\psi$, a nonzero expectation value of O implies that the state under investigation is in the GHZ class [31]. To further categorize the classes of three-qubit generic states we need three more observables $O_1 = 2\sigma_x^1\sigma_x^2\sigma_z^3$, $O_2 = 2\sigma_x^1\sigma_z^2\sigma_x^3$, $O_3 = 2\sigma_z^1\sigma_x^2\sigma_x^3$. Experimentally measuring the expectation values of the operators O, O_1, O_2, and O_3 can reveal the entanglement class of every three-qubit pure state [34,35]. Table I summarizes the classification of the six SLOCC inequivalent classes of entangled states based on the expectation values of the observables O, O_1, O_2, O_3. The six SLOCC inequivalent classes of three-qubit entangled states are GHZ, W, BS_1, BS_2, BS_3, and separable. While GHZ and W classes are well known, BS_1 denotes a biseparable class having B and C subsystems entangled, the BS_2 class has subsystems A and C entangled, while the BS_3 class has subsystems A and B entangled. As has been summarized in Table I, a nonzero value of $\langle O\rangle$ indicates that the state is in the GHZ class and this expectation value is zero for all other classes. For the W class of states, all $\langle O_j\rangle$ are nonzero except $\langle O\rangle$. For the BS_1 class only $\langle O_3\rangle$ is nonzero while only $\langle O_2\rangle$ and $\langle O_1\rangle$ are nonzero for the classes BS_2 and BS_3, respectively. For separable states all expectations are zero.

TABLE I. Decision table for the classification of three-qubit pure entangled states based on the expectation values of operators O, O_1, O_2, and O_3 in state $|\psi\rangle$. Each class in the row is shown with the expected values of the observables.

Class	$\langle O\rangle$	$\langle O_1\rangle$	$\langle O_2\rangle$	$\langle O_3\rangle$
GHZ	$\neq 0$	[a]	[a]	[a]
W	0	$\neq 0$	$\neq 0$	$\neq 0$
BS_1	0	0	0	$\neq 0$
BS_2	0	0	$\neq 0$	0
BS_3	0	$\neq 0$	0	0
Separable	0	0	0	0

[a]May or may not be zero.

To experimentally realize the entanglement characterization protocol, one has to determine the expectation values $\langle O\rangle$, $\langle O_1\rangle$, $\langle O_2\rangle$, and $\langle O_3\rangle$ for an experimentally prepared state $|\psi\rangle$. In the next section we describe our method to experimentally realize these expectation values based on subsystem measurement of the Pauli z operator [36] and our experimental scheme for generating arbitrary three-qubit states [14].

Mapping Pauli-basis operators to single-qubit z operators

A standard way to determine the expectation value of a desired observable in an experiment is to decompose the observable as a linear superposition of the observables accessible in the experiment [41]. This task becomes particularly accessible while dealing with the Pauli basis.

Any observable for a three-qubit system acting on an eight-dimensional Hilbert space can be decomposed as a linear superposition of 64 basis operators, and the Pauli basis is one possible basis for this decomposition. Let the set of Pauli basis operators be denoted $\mathbb{B} = \{\mathrm{B_i}; 0 \leqslant \mathrm{i} \leqslant 63\}$. For example, O_2 has the form $\sigma_x^1\sigma_z^2\sigma_x^3$ and is element B_{29} of the basis set $\mathbb{B}$. The four observables O, O_1, O_2, and O_3 are represented by the elements B_{21}, B_{23}, B_{29}, and B_{53}, respectively, of the Pauli basis set $\mathbb{B}$. Also by this convention the single-qubit z operators for the first, second, and third qubit, i.e., σ_z^1, σ_z^2, and σ_z^3 are the elements B_{48}, B_{12}, and B_3, respectively.

Table II details the mapping of all 63 Pauli basis operators (excluding the $8 \otimes 8$ identity operator) to the single-qubit Pauli z operator. This mapping is particularly useful in an experimental setup where the expectation values of Pauli's local z operators are easily accessible. In NMR experiments, the z magnetization of a nuclear spin in a state is proportional

TABLE II. All 63 product operators, for a three-spin (half) system, mapped to the Pauli z operators (of either spin 1, spin 2, or spin 3) by mapping the initial state $\rho \to \rho_i = U_i \cdot \rho \cdot U_i^\dagger$.

Observable	Initial state mapped via	Observable	Initial state mapped via
$\langle B_1\rangle = \mathrm{Tr}[\rho_1 \cdot I_z^3]$	$U_1 = \overline{Y}_3$	$\langle B_{33}\rangle = \mathrm{Tr}[\rho_{33} \cdot I_z^3]$	$U_{33} = \mathrm{CNOT}_{13} \cdot \overline{Y}_3 \cdot X_1$
$\langle B_2\rangle = \mathrm{Tr}[\rho_2 \cdot I_z^3]$	$U_2 = X_3$	$\langle B_{34}\rangle = \mathrm{Tr}[\rho_{34} \cdot I_z^3]$	$U_{34} = \mathrm{CNOT}_{13} \cdot X_3 \cdot X_1$
$\langle B_3\rangle = \mathrm{Tr}[\rho_3 \cdot I_z^3]$	$U_3 = \mathbb{I}_8$	$\langle B_{35}\rangle = \mathrm{Tr}[\rho_{35} \cdot I_z^3]$	$U_{35} = \mathrm{CNOT}_{13} \cdot X_1$
$\langle B_4\rangle = \mathrm{Tr}[\rho_4 \cdot I_z^2]$	$U_4 = \overline{Y}_2$	$\langle B_{36}\rangle = \mathrm{Tr}[\rho_{36} \cdot I_z^2]$	$U_{36} = \mathrm{CNOT}_{12} \cdot \overline{Y}_2 \cdot X_1$
$\langle B_5\rangle = \mathrm{Tr}[\rho_5 \cdot I_z^3]$	$U_5 = \mathrm{CNOT}_{23} \cdot \overline{Y}_3 \cdot \overline{Y}_2$	$\langle B_{37}\rangle = \mathrm{Tr}[\rho_{37} \cdot I_z^3]$	$U_{37} = \mathrm{CNOT}_{23} \cdot \overline{Y}_3 \cdot \mathrm{CNOT}_{12} \cdot \overline{Y}_2 \cdot X_1$
$\langle B_6\rangle = \mathrm{Tr}[\rho_6 \cdot I_z^3]$	$U_6 = \mathrm{CNOT}_{23} \cdot X_3 \cdot \overline{Y}_2$	$\langle B_{38}\rangle = \mathrm{Tr}[\rho_{38} \cdot I_z^3]$	$U_{38} = \mathrm{CNOT}_{23} \cdot X_3 \cdot \mathrm{CNOT}_{12} \cdot \overline{Y}_2 \cdot X_1$
$\langle B_7\rangle = \mathrm{Tr}[\rho_7 \cdot I_z^3]$	$U_7 = \mathrm{CNOT}_{23} \cdot \overline{Y}_2$	$\langle B_{39}\rangle = \mathrm{Tr}[\rho_{39} \cdot I_z^3]$	$U_{39} = \mathrm{CNOT}_{23} \cdot \mathrm{CNOT}_{12} \cdot \overline{Y}_2 \cdot X_1$
$\langle B_8\rangle = \mathrm{Tr}[\rho_8 \cdot I_z^2]$	$U_8 = X_2$	$\langle B_{40}\rangle = \mathrm{Tr}[\rho_{40} \cdot I_z^2]$	$U_{40} = \mathrm{CNOT}_{12} \cdot X_2 \cdot X_1$
$\langle B_9\rangle = \mathrm{Tr}[\rho_9 \cdot I_z^3]$	$U_9 = \mathrm{CNOT}_{23} \cdot \overline{Y}_3 \cdot X_2$	$\langle B_{41}\rangle = \mathrm{Tr}[\rho_{41} \cdot I_z^3]$	$U_{41} = \mathrm{CNOT}_{23} \cdot \overline{Y}_3 \cdot \mathrm{CNOT}_{12} \cdot X_2 \cdot X_1$
$\langle B_{10}\rangle = \mathrm{Tr}[\rho_{10} \cdot I_z^3]$	$U_{10} = \mathrm{CNOT}_{23} \cdot X_3 \cdot X_2$	$\langle B_{42}\rangle = \mathrm{Tr}[\rho_{42} \cdot I_z^3]$	$U_{42} = \mathrm{CNOT}_{23} \cdot X_3 \cdot \mathrm{CNOT}_{12} \cdot X_2 \cdot X_1$
$\langle B_{11}\rangle = \mathrm{Tr}[\rho_{11} \cdot I_z^3]$	$U_{11} = \mathrm{CNOT}_{23} \cdot X_2$	$\langle B_{43}\rangle = \mathrm{Tr}[\rho_{43} \cdot I_z^3]$	$U_{43} = \mathrm{CNOT}_{23} \cdot \mathrm{CNOT}_{12} \cdot X_2 \cdot X_1$
$\langle B_{12}\rangle = \mathrm{Tr}[\rho_{12} \cdot I_z^3]$	$U_{12} = \mathbb{I}_8$	$\langle B_{44}\rangle = \mathrm{Tr}[\rho_{44} \cdot I_z^2]$	$U_{44} = \mathrm{CNOT}_{12} \cdot X_1$
$\langle B_{13}\rangle = \mathrm{Tr}[\rho_{13} \cdot I_z^3]$	$U_{13} = \mathrm{CNOT}_{23} \cdot \overline{Y}_3$	$\langle B_{45}\rangle = \mathrm{Tr}[\rho_{45} \cdot I_z^3]$	$U_{45} = \mathrm{CNOT}_{23} \cdot \overline{Y}_3 \cdot \mathrm{CNOT}_{12} \cdot X_1$
$\langle B_{14}\rangle = \mathrm{Tr}[\rho_{14} \cdot I_z^3]$	$U_{14} = \mathrm{CNOT}_{23} \cdot X_3$	$\langle B_{46}\rangle = \mathrm{Tr}[\rho_{46} \cdot I_z^3]$	$U_{46} = \mathrm{CNOT}_{23} \cdot X_3 \cdot \mathrm{CNOT}_{12} \cdot X_1$
$\langle B_{15}\rangle = \mathrm{Tr}[\rho_{15} \cdot I_z^3]$	$U_{15} = \mathrm{CNOT}_{23}$	$\langle B_{47}\rangle = \mathrm{Tr}[\rho_{47} \cdot I_z^3]$	$U_{47} = \mathrm{CNOT}_{23} \cdot \mathrm{CNOT}_{12} \cdot X_1$
$\langle B_{16}\rangle = \mathrm{Tr}[\rho_{16} \cdot I_z^1]$	$U_{16} = X_1$	$\langle B_{48}\rangle = \mathrm{Tr}[\rho_{48} \cdot I_z^1]$	$U_{48} = \mathbb{I}_8$
$\langle B_{17}\rangle = \mathrm{Tr}[\rho_{17} \cdot I_z^3]$	$U_{17} = \mathrm{CNOT}_{13} \cdot \overline{Y}_3 \cdot \overline{Y}_1$	$\langle B_{49}\rangle = \mathrm{Tr}[\rho_{49} \cdot I_z^3]$	$U_{49} = \mathrm{CNOT}_{13} \cdot \overline{Y}_3$
$\langle B_{18}\rangle = \mathrm{Tr}[\rho_{18} \cdot I_z^3]$	$U_{18} = \mathrm{CNOT}_{13} \cdot X_3 \cdot \overline{Y}_1$	$\langle B_{50}\rangle = \mathrm{Tr}[\rho_{50} \cdot I_z^3]$	$U_{50} = \mathrm{CNOT}_{13} \cdot X_3$
$\langle B_{19}\rangle = \mathrm{Tr}[\rho_{19} \cdot I_z^3]$	$U_{19} = \mathrm{CNOT}_{13} \cdot \overline{Y}_1$	$\langle B_{51}\rangle = \mathrm{Tr}[\rho_{51} \cdot I_z^3]$	$U_{51} = \mathrm{CNOT}_{13}$
$\langle B_{20}\rangle = \mathrm{Tr}[\rho_{20} \cdot I_z^2]$	$U_{20} = \mathrm{CNOT}_{12} \cdot \overline{Y}_2 \cdot \overline{Y}_1$	$\langle B_{52}\rangle = \mathrm{Tr}[\rho_{52} \cdot I_z^2]$	$U_{52} = \mathrm{CNOT}_{12} \cdot \overline{Y}_2$
$\langle B_{21}\rangle = \mathrm{Tr}[\rho_{21} \cdot I_z^3]$	$U_{21} = \mathrm{CNOT}_{23} \cdot \overline{Y}_3 \cdot \mathrm{CNOT}_{12} \cdot \overline{Y}_2 \cdot \overline{Y}_1$	$\langle B_{53}\rangle = \mathrm{Tr}[\rho_{53} \cdot I_z^3]$	$U_{53} = \mathrm{CNOT}_{23} \cdot \overline{Y}_3 \cdot \mathrm{CNOT}_{12} \cdot \overline{Y}_2$
$\langle B_{22}\rangle = \mathrm{Tr}[\rho_{22} \cdot I_z^3]$	$U_{22} = \mathrm{CNOT}_{23} \cdot X_3 \cdot \mathrm{CNOT}_{12} \cdot \overline{Y}_2 \cdot \overline{Y}_1$	$\langle B_{54}\rangle = \mathrm{Tr}[\rho_{54} \cdot I_z^3]$	$U_{54} = \mathrm{CNOT}_{23} \cdot X_3 \cdot \mathrm{CNOT}_{12} \cdot \overline{Y}_2$
$\langle B_{23}\rangle = \mathrm{Tr}[\rho_{23} \cdot I_z^3]$	$U_{23} = \mathrm{CNOT}_{23} \cdot \mathrm{CNOT}_{12} \cdot \overline{Y}_2 \cdot \overline{Y}_1$	$\langle B_{55}\rangle = \mathrm{Tr}[\rho_{55} \cdot I_z^3]$	$U_{55} = \mathrm{CNOT}_{23} \cdot \mathrm{CNOT}_{12} \cdot \overline{Y}_2$
$\langle B_{24}\rangle = \mathrm{Tr}[\rho_{24} \cdot I_z^2]$	$U_{24} = \mathrm{CNOT}_{12} \cdot X_2 \cdot \overline{Y}_1$	$\langle B_{56}\rangle = \mathrm{Tr}[\rho_{56} \cdot I_z^2]$	$U_{56} = \mathrm{CNOT}_{12} \cdot X_2$
$\langle B_{25}\rangle = \mathrm{Tr}[\rho_{25} \cdot I_z^3]$	$U_{25} = \mathrm{CNOT}_{23} \cdot \overline{Y}_3 \cdot \mathrm{CNOT}_{12} \cdot X_2 \cdot \overline{Y}_1$	$\langle B_{57}\rangle = \mathrm{Tr}[\rho_{57} \cdot I_z^3]$	$U_{57} = \mathrm{CNOT}_{23} \cdot \overline{Y}_3 \cdot \mathrm{CNOT}_{12} \cdot X_2$
$\langle B_{26}\rangle = \mathrm{Tr}[\rho_{26} \cdot I_z^3]$	$U_{26} = \mathrm{CNOT}_{23} \cdot X_3 \cdot \mathrm{CNOT}_{12} \cdot X_2 \cdot \overline{Y}_1$	$\langle B_{58}\rangle = \mathrm{Tr}[\rho_{58} \cdot I_z^3]$	$U_{58} = \mathrm{CNOT}_{23} \cdot X_3 \cdot \mathrm{CNOT}_{12} \cdot X_2$
$\langle B_{27}\rangle = \mathrm{Tr}[\rho_{27} \cdot I_z^3]$	$U_{27} = \mathrm{CNOT}_{23} \cdot \mathrm{CNOT}_{12} \cdot X_2 \cdot \overline{Y}_1$	$\langle B_{59}\rangle = \mathrm{Tr}[\rho_{59} \cdot I_z^3]$	$U_{59} = \mathrm{CNOT}_{23} \cdot \mathrm{CNOT}_{12} \cdot X_2$
$\langle B_{28}\rangle = \mathrm{Tr}[\rho_{28} \cdot I_z^2]$	$U_{28} = \mathrm{CNOT}_{12} \cdot \overline{Y}_1$	$\langle B_{60}\rangle = \mathrm{Tr}[\rho_{60} \cdot I_z^2]$	$U_{60} = \mathrm{CNOT}_{12}$
$\langle B_{29}\rangle = \mathrm{Tr}[\rho_{29} \cdot I_z^3]$	$U_{29} = \mathrm{CNOT}_{23} \cdot \overline{Y}_3 \cdot \mathrm{CNOT}_{12} \cdot \overline{Y}_1$	$\langle B_{61}\rangle = \mathrm{Tr}[\rho_{61} \cdot I_z^3]$	$U_{61} = \mathrm{CNOT}_{23} \cdot \overline{Y}_3 \cdot \mathrm{CNOT}_{12}$
$\langle B_{30}\rangle = \mathrm{Tr}[\rho_{30} \cdot I_z^3]$	$U_{30} = \mathrm{CNOT}_{23} \cdot X_3 \cdot \mathrm{CNOT}_{12} \cdot \overline{Y}_1$	$\langle B_{62}\rangle = \mathrm{Tr}[\rho_{62} \cdot I_z^3]$	$U_{62} = \mathrm{CNOT}_{23} \cdot X_3 \cdot \mathrm{CNOT}_{12}$
$\langle B_{31}\rangle = \mathrm{Tr}[\rho_{31} \cdot I_z^3]$	$U_{31} = \mathrm{CNOT}_{12} \cdot \mathrm{CNOT}_{23} \cdot \overline{Y}_1$	$\langle B_{63}\rangle = \mathrm{Tr}[\rho_{63} \cdot I_z^3]$	$U_{63} = \mathrm{CNOT}_{23} \cdot \mathrm{CNOT}_{12}$
$\langle B_{32}\rangle = \mathrm{Tr}[\rho_{32} \cdot I_z^1]$	$U_{32} = X_1$		

to the expectation value of Pauli z operator of that spin in the state.

As an example of the mapping given in Table II, the operator O_2 has the form $\sigma_x^1\sigma_z^2\sigma_x^3$ and is the element B_{29} of basis set $\mathbb{B}$. It should be noted here that the order of the basis elements in the Table II is in the increasing order of base-four subscript, since in the base-four notation, 0, 1, 2, 3 can be directly mapped to either identity or Pauli x, y, and z matrices (for details see the convention followed in Ref. [42]). To determine $\langle O_2\rangle$ in the state $\rho = |\psi\rangle\langle\psi|$, one can map the state $\rho \to \rho_{29} = U_{29} \cdot \rho \cdot U_{29}^\dagger$ with $U_{29} = \mathrm{CNOT}_{23} \cdot \overline{Y}_3 \cdot \mathrm{CNOT}_{12} \cdot \overline{Y}_1$. This is followed by finding $\langle\sigma_z^3\rangle$ in the state ρ_{29}. The expectation value $\langle\sigma_z^3\rangle$ in the state ρ_{29} is equivalent to the expectation value of $\langle O_2\rangle$ in the state $\rho = |\psi\rangle\langle\psi|$ (Table II); the operation CNOT_{kl} is a controlled-NOT gate with k as the control qubit and l as the target qubit, and X, $\overline{X}$, Y, and $\overline{Y}$ represent local $\frac{\pi}{2}$ unitary rotations with phases x, $-x$, y, and $-y$, respectively. The subscript on $\pi/2$ local unitary rotations denotes qubit number. The quantum circuit to achieve such a mapping is shown in Fig. 1(a).

Note that, while measuring the expectation values of O, O_1, O_2, or O_3, all the $\overline{Y}$ local rotations may not act in all four of these cases. The mapping given in Table II is used to decide which $\overline{Y}$ local rotation in the circuit 1(a) will act. All the basis operators in set $\mathbb{B}$ can be mapped to single-qubit z operators in a similar fashion. The mapping given in Table II is not unique and there are several equivalent mappings which can be worked out as per the experimental requirements.

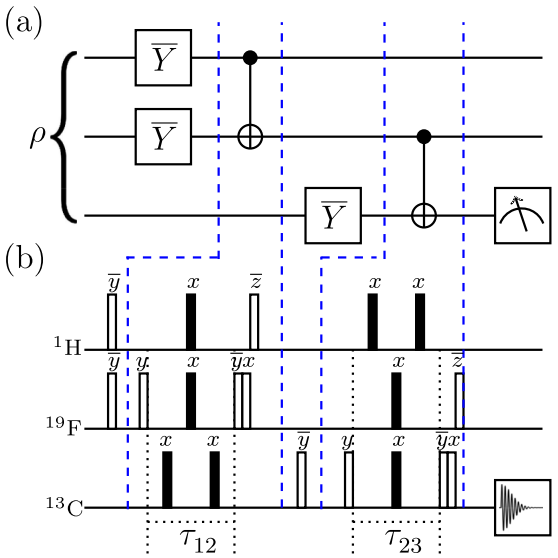

FIG. 1. (a) Quantum circuit to achieve mapping of the state ρ to either of the states ρ_{21}, ρ_{23}, ρ_{29}, or ρ_{53} followed by measurement of qubit three in the computational basis. (b) NMR pulse sequence of the quantum circuit given in panel (a). All the unfilled rectangles denote $\frac{\pi}{2}$ spin-selective rf pulses while filled rectangles denote π pulses. Pulse phases are written above the respective pulse and a bar over a phase represents negative phase. Delays are given by $\tau_{ij} = 1/(8J_{ij})$; i, j label the qubit and J is the coupling constant.

III. NMR IMPLEMENTATION OF THREE-QUBIT ENTANGLEMENT DETECTION PROTOCOL

The Hamiltonian [43] for a three-qubit system in the rotating frame is given by

$$\mathcal{H} = -\sum_{i=1}^{3} \nu_i I_z^i + \sum_{i>j,i=1}^{3} J_{ij} I_z^i I_z^j, \tag{4}$$

where the indices i, $j = 1$, 2, or 3 represent the qubit number and ν_i is the respective chemical shift in rotating frame, J_{ij} is the scalar coupling constant, and I_z^i is the Pauli's z-spin angular-momentum operator of the ith qubit. To implement the entanglement detection protocol experimentally, ^{13}C-labeled diethyl fluoromalonate dissolved in an acetone-D6 sample was used. ^{1}H, ^{19}F, and ^{13}C spin-half nuclei were encoded as qubit one, qubit two, and qubit three, respectively. The system was initialized in the pseudopure (PPS) state, i.e., $|000\rangle$, using the spatial averaging [44,45] with the density operator being

$$\rho_{000} = \frac{1-\epsilon}{2^3}\mathbb{I}_8 + \epsilon|000\rangle\langle 000|, \tag{5}$$

where $\epsilon \sim 10^{-5}$ is the thermal polarization at room temperature and $\mathbb{I}_8$ is the 8×8 identity operator. The experimentally determined NMR parameters (chemical shifts, T_1 and T_2 relaxation times, and scalar couplings J_{ij}) as well as the NMR spectra of the PPS state are shown in Fig. 2. Each spectral transition is labeled with the logical states of the passive qubits (i.e., qubits not undergoing any transition) in the computational basis. The state fidelity of the experimentally prepared PPS [Fig. 2(c)] was compute to be 0.98 ± 0.01 and

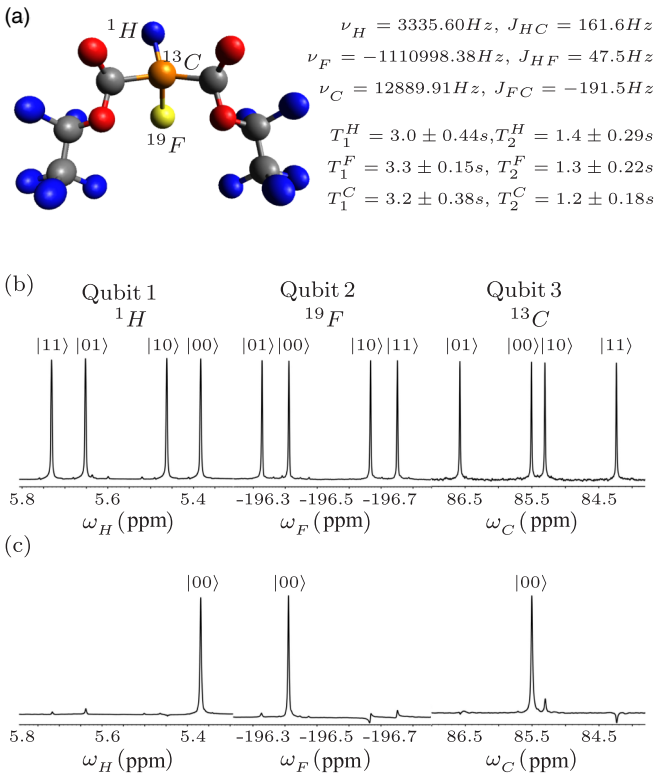

FIG. 2. (a) Molecular structure of ^{13}C-labeled diethyl fluoromalonate and NMR parameters. NMR spectra of (b) thermal equilibrium state and (c) pseudopure state. Each peak is labeled with the logical state of the qubit which is passive during the transition. Horizontal scale represents the chemical shifts in ppm.

was calculated by using the fidelity measure [46,47]

$$F = [\mathrm{Tr}(\sqrt{\sqrt{\rho_{\mathrm{theor}}}\rho_{\mathrm{expt}}\sqrt{\rho_{\mathrm{theor}}}})]^2, \tag{6}$$

where ρ_{theor} and ρ_{expt} are the theoretically expected and the experimentally reconstructed density operators, respectively. Fidelity measure is normalized such that $F \to 1$ as $\rho_{\mathrm{expt}} \to \rho_{\mathrm{theor}}$. For the experimental reconstruction of density operator, full quantum state tomography (QST) [42,48] was performed by using a preparatory pulse set

$$\{III, XXX, IIY, XYX, YII, XXY, IYY\},$$

where I implies "no operation." In NMR, a $\frac{\pi}{2}$ local unitary rotation X (Y) can be achieved by using spin-selective transverse radio frequency (rf) pulses having phase x (y).

Experiments were performed at room temperature (293 K) on a Bruker Avance III 600-MHz FT-NMR spectrometer equipped with a QXI probe. Local unitary operations were achieved by using highly accurate and calibrated spin-selective transverse rf pulses of suitable amplitude, phase, and duration. Nonlocal unitary operation were achieved by free evolution under the system Hamiltonian (4), of suitable duration under the desired scalar coupling with the help of embedded π refocusing pulses. In the current study, the durations of $\frac{\pi}{2}$ pulses for ^{1}H, ^{19}F, and ^{13}C were 9.55 μs at 18.14 W power level, 22.80 μs at a power level of 42.27 W, and 15.50 μs at a power level of 179.47 W, respectively.

A. Measuring observables by mapping to local z magnetization

As discussed in Sec. II, the observables required to differentiate between six inequivalent classes of three-qubit pure entangled states can be mapped to the Pauli z operator of one of the qubits. Furthermore, in NMR, the observed z magnetization of a nuclear spin in a quantum state is proportional to the expectation value of the σ_z operator [43] of the spin in that state. The time-domain NMR signal, i.e., the free-induction decay with appropriate phase gives Lorentzian peaks when Fourier transformed. These normalized experimental intensities give an estimate of the expectation value of σ_z of the quantum state.

Let $\hat{\mathcal{O}}$ be the observable whose expectation value is to be measured in a state $\rho = |\psi\rangle\langle\psi|$. Instead of measuring $\langle\hat{\mathcal{O}}\rangle_\rho$, the state ρ can be mapped to ρ_i by using $\rho_i = U_i.\rho.U_i^\dagger$ followed by a z-magnetization measurement of one of the qubits. Table II lists the explicit forms of U_i for all the basis elements of the Pauli basis set $\mathbb{B}$. In the present study, the observables of interest are O, O_1, O_2, and O_3, as described in Sec. II and Table I. The quantum circuit to achieve the required mapping is shown in Fig. 1(a). The circuit is designed to map the state ρ to either of the states ρ_{21}, ρ_{23}, ρ_{29}, or ρ_{53} followed by a σ_z measurement on the third qubit, i.e., σ_z^3, in the mapped state. Depending on the experimental settings, $\langle B_3\rangle$ in the mapped states is indeed the expectation values of O, O_1, O_2, or O_3 in the initial state ρ.

The NMR pulse sequence to achieve the quantum mapping of circuit in Fig. 1(a) is shown in Fig. 1(b). The unfilled rectangles represent $\frac{\pi}{2}$ spin-selective pulses while the filled rectangles represent π pulses. Evolution under chemical shifts has been refocused during all the free evolution periods (denoted by $\tau_{ij} = \frac{1}{8J_{ij}}$) and π pulses are embedded between the free evolution periods in such a way that the system evolves only under the desired scalar coupling J_{ij}.

B. Implementing the entanglement detection protocol

The three-qubit system was prepared in 27 different states in order to experimentally demonstrate the efficacy of the entanglement detection protocol. Seven representative states were prepared from the six inequivalent entanglement classes, i.e., GHZ (GHZ and $W\overline{W}$ states), W, three biseparable and a separable class of states. In addition, 20 generic states were randomly generated (labeled as R_1, R_2, R_3, …, R_{20}). Our recent [14] experimental scheme was utilized to prepare the generic three-qubit states. For the details of quantum circuits as well as NMR pulse sequences used for state preparation, see Ref. [14]. All the prepared states had state fidelities ranging between 0.89 to 0.99. Each prepared state ρ was passed through the detection circuit 1(a) to yield the expectation values of the observables O, O_1, O_2, and O_3, as described in Sec. III A. Furthermore, full QST [44] was performed to directly estimate the expectation value of O, O_1, O_2, and O_3 for all the 27 states.

The results of the experimental implementation of the three-qubit entanglement detection protocol are tabulated in Table III. For a visual representation of the data in Table III, bar charts are shown in Fig. 3. The seven known states were numbered as 1–7 while the 20 random states were numbered as 8–27, in accordance with Table III. Horizontal axes in plots of Fig. 3 denote the state number while vertical axes represent the value of the respective observable. Black, cross-hatched, and unfilled bars represent theoretical (The.), direct (Dir.) experimental, and QST-based expectation values, respectively. To further quantify the entanglement quotient, the entanglement measure, negativity [49,50] was also computed theoretically as well as experimentally in all the cases (Table IV). Experiments were repeated several times for error estimation and to validate the reproducibility of the experimental results. All the seven representative states belonging to the six inequivalent entanglement classes were detected successfully within the experimental error limits, as suggested by the experimental results in the first seven rows of Table III in comparison with Table I. The errors in the experimental expectation values reported in the Table III were in the range 3.1%–8.5%. The entanglement detection protocol with only four observables is further supported by negativity measurements (Table IV). Note here that one will never be able to conclude that the result of an experimental observation

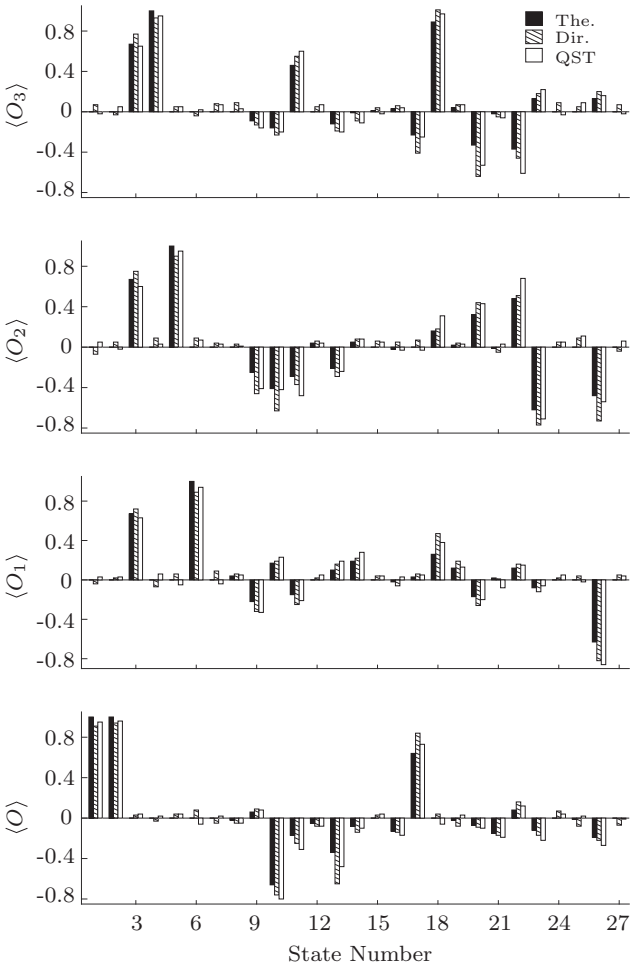

FIG. 3. Bar plots of the expectation values of the observables O, O_1, O_2, and O_3 for states numbered from 1–27 (Table III). The horizontal axes denote the state number while the vertical axes represent the values of the respective observable. Black, cross-hatched, and unfilled bars represent the theoretical (The.), directly (Dir.) measured from experiment, and QST-derived expectation values, respectively.

TABLE III. Results of the three-qubit entanglement detection protocol for 27 states. The label BS is for biseparable states and R is for random states. The first column depicts the state label, the top row lists the observable (Obs.), while second row specify if the observable value is theoretical (The.), direct experimental (Dir.), or from QST.

Obs. →	$\langle O\rangle$			$\langle O_1\rangle$			$\langle O_2\rangle$			$\langle O_3\rangle$		
State(F) ↓	The.	Dir.	QST	The.	Dir.	QST	The.	Dir.	QST	The.	Dir.	QST
GHZ(0.95 ± 0.03)	1.00	0.91	0.95	0	−0.04	0.03	0	−0.07	0.05	0	0.07	−0.02
$W\overline{W}$(0.98 ± 0.01)	1.00	0.94	0.96	0	0.02	0.03	0	0.05	−0.02	0	−0.03	0.05
W(0.96 ± 0.02)	0	0.05	0.04	0.67	0.60	0.62	0.67	0.61	0.69	0.67	0.59	0.63
BS_1(0.95 ± 0.02)	0	−0.03	0.02	0	−0.07	0.06	0	0.09	0.03	1.00	0.93	0.95
BS_2(0.96 ± 0.03)	0	0.04	0.04	0	0.06	−0.05	1.00	0.90	0.95	0	0.05	0.05
BS_3(0.95 ± 0.04)	0	0.08	−0.06	1.00	0.89	0.94	0	0.09	0.07	0	−0.04	0.02
Sep(0.98 ± 0.01)	0	−0.05	0.02	0	0.09	−0.04	0	0.04	0.03	0	0.08	0.07
R_1(0.91 ± 0.02)	−0.02	−0.05	−0.05	0.04	0.06	0.05	0.00	0.03	0.01	0.00	0.09	0.03
R_2(0.94 ± 0.03)	0.06	0.09	0.08	−0.22	−0.32	−0.33	−0.25	−0.46	−0.41	−0.09	−0.13	−0.16
R_3(0.93 ± 0.03)	−0.66	−0.76	−0.80	0.17	0.19	0.23	−0.41	−0.63	−0.42	−0.16	−0.23	−0.20
R_4(0.91 ± 0.01)	−0.17	−0.25	−0.31	−0.15	−0.25	−0.21	−0.29	−0.37	−0.48	0.46	0.55	0.60
R_5(0.94 ± 0.03)	−0.05	−0.08	−0.08	0.00	0.02	0.05	0.04	0.06	0.04	0.00	0.05	0.07
R_6(0.90 ± 0.02)	−0.34	−0.65	−0.48	0.10	0.16	0.19	−0.21	−0.29	−0.24	−0.12	−0.19	−0.20
R_7(0.93 ± 0.03)	−0.08	−0.14	−0.10	0.19	0.22	0.28	0.05	0.08	0.08	−0.01	−0.09	−0.11
R_8(0.94 ± 0.01)	0.00	0.03	0.04	0.00	0.04	0.04	0.00	0.06	0.05	0.01	0.04	−0.02
R_9(0.95 ± 0.02)	−0.13	−0.14	−0.17	−0.02	−0.06	0.03	−0.02	0.05	−0.03	0.03	0.06	0.04
R_{10}(0.92 ± 0.03)	0.64	0.84	0.73	0.03	0.06	0.05	0.00	0.07	−0.03	−0.23	−0.41	−0.25
R_{11}(0.93 ± 0.03)	0.00	0.04	−0.06	0.26	0.47	0.38	0.16	0.18	0.31	0.89	1.01	0.97
R_{12}(0.89 ± 0.02)	−0.02	−0.08	0.03	0.12	0.19	0.13	0.02	0.04	0.03	0.04	0.07	0.07
R_{13}(0.92 ± 0.03)	−0.07	−0.09	−0.10	−0.17	−0.26	−0.20	0.32	0.44	0.43	−0.33	−0.64	−0.53
R_{14}(0.94 ± 0.04)	−0.15	−0.17	−0.19	0.02	0.01	−0.08	−0.01	−0.05	0.03	−0.02	−0.05	−0.06
R_{15}(0.94 ± 0.03)	0.08	0.16	0.12	0.12	0.16	0.15	0.48	0.51	0.68	−0.37	−0.46	−0.61
R_{16}(0.93 ± 0.02)	−0.12	−0.17	−0.22	−0.08	−0.12	−0.06	−0.62	−0.77	−0.71	0.13	0.18	0.22
R_{17}(0.93 ± 0.04)	0.00	0.07	0.04	0.00	0.02	0.05	0.00	0.05	0.05	0.00	0.09	−0.03
R_{18}(0.90 ± 0.02)	−0.01	−0.08	0.02	0.00	0.04	−0.02	0.00	0.09	0.11	0.00	0.05	0.09
R_{19}(0.94 ± 0.02)	−0.19	−0.22	−0.27	−0.63	−0.82	−0.86	−0.48	−0.73	−0.54	0.13	0.20	0.16
R_{20}(0.93 ± 0.03)	0.00	−0.07	−0.01	0.00	0.05	0.04	0.00	−0.04	0.06	0.00	0.07	−0.02

is exactly zero. However, it can be established that the result is nonzero. This has to be kept in mind while interpreting the experimentally obtained values of the operators involved via the decision Table I.

The results for the 20 randomly generated generic states, numbered 8–27 (R_1–R_{20}) are interesting. For instance, states R_{10} and R_{11} have a negativity of approximately 0.35 which implies that these states have genuine tripartite entanglement. On the other hand, the experimental results of the current detection protocol (Table III) suggest that R_{10} has a nonzero three-tangle, which is a signature of the GHZ class. The states R_3, R_4, R_6, R_7, R_{14}, R_{16}, and R_{19} also belong to the GHZ class because they all have nonzero three-tangle as well as finite negativity. On the other hand, the state R_{11} has a vanishing three-tangle with nonvanishing expectation values of O_1, O_2, and O_3 which indicates that this state belongs to the W class. The states R_2, R_{13}, and R_{15} were also identified as members of the W class by using the detection protocol. These results demonstrate the fine-grained state discrimination power of the entanglement detection protocol as compared with procedures that rely on QST. Furthermore, all vanishing expectation values as well as a near-zero negativity, in the case of the R_8 state, imply that it belongs to the separable class. The randomly generated states R_1, R_5, R_{17}, R_{18}, and R_{20} have also been identified as belonging to the separable class of states. Interestingly, R_{12} has vanishing values of three-tangle, negativity, $\langle O_2\rangle$, and $\langle O_3\rangle$ but has a finite value of $\langle O_1\rangle$, from which one can conclude that this state belongs to the biseparable BS_3 class.

C. Effect of mixedness in the prepared states

While the proposed entanglement classification protocol assumes the state under investigation to be pure, the experimentally prepared states are invariably mixed. The experimentally prepared density operator ρ_e can be expanded in terms of its eigenvalues λ_j and corresponding eigenvectors $|\lambda_j\rangle$ as $\rho_e = \sum_{j=1}^{8} |\lambda_j\rangle\langle\lambda_j|$, obeying the normalization condition $\sum_{j=1}^{8} \lambda_j = 1$. For a pure state ρ_p, only one of the eigenvalues can be nonzero, so we take $\lambda_1^p = 1$ and the other eigenvalues to be zero. The expectation value of the observable $\hat{\mathcal{O}}$ can then

TABLE IV. Theoretically calculated and experimentally measured values of negativity.

Negativity → State ↓	Theoretical	Experimental
GHZ	0.5	0.46 ± 0.03
$W\overline{W}$	0.37	0.35 ± 0.03
W	0.47	0.41 ± 0.02
BS_1	0	0.03 ± 0.02
BS_2	0	0.05 ± 0.02
BS_3	0	0.03 ± 0.03
Sep	0	0.02 ± 0.01
R_1	0.02	0.04 ± 0.02
R_2	0.16	0.12 ± 0.04
R_3	0.38	0.35 ± 0.07
R_4	0.38	0.34 ± 0.06
R_5	0.03	0.04 ± 0.02
R_6	0.21	0.18 ± 0.04
R_7	0.09	0.08 ± 0.03
R_8	0	0.02 ± 0.02
R_9	0.07	0.06 ± 0.03
R_{10}	0.38	0.35 ± 0.08
R_{11}	0.32	0.28 ± 0.06
R_{12}	0.05	0.04 ± 0.02
R_{13}	0.18	0.15 ± 0.03
R_{14}	0.08	0.07 ± 0.02
R_{15}	0.34	0.32 ± 0.06
R_{16}	0.30	0.28 ± 0.06
R_{17}	0	0.03 ± 0.02
R_{18}	0	0.02 ± 0.02
R_{19}	0.39	0.36 ± 0.09
R_{20}	0	0.02 ± 0.02

be written as

$$\langle \hat{\mathcal{O}} \rangle_p = \left\langle \lambda_1^p \middle| \hat{\mathcal{O}} \middle| \lambda_1^p \right\rangle = \mathrm{Tr}[\rho_p \cdot \hat{\mathcal{O}}]. \tag{7}$$

In an actual experiment the situation is different and several eigenvalues of the density operator may be nonzero. The errors can arise either from the mixedness present in the experimentally prepared state ρ_e or in the experimental measurement of $\langle \hat{\mathcal{O}} \rangle$. These errors are dominantly caused by imperfections in the unitary rotations used in state preparation, rf inhomogeneity of the applied magnetic field, as well as T_2 and T_1 decoherence processes.

Let λ_1 be the maximum eigenvalue of the experimentally prepared state ρ_e. Mixedness is indicated by nonzero eigenvalues λ_j for $j \neq 1$. The expectation value of $\hat{\mathcal{O}}$ can be written as an equation similar to Eq. (7):

$$\langle \hat{\mathcal{O}} \rangle e = \mathrm{Tr}[\rho_e . \hat{\mathcal{O}}] = \sum_{j=1}^{8} \lambda_i \mathrm{Tr}[P_i . \hat{\mathcal{O}}] = \sum_{j=1}^{8} \lambda_i o_i. \tag{8}$$

The question is that, if we approximate our state to be a pure state corresponding to the largest eigenvalue λ_1 and take $\langle \hat{\mathcal{O}} \rangle_p = \langle \lambda_1 | \hat{\mathcal{O}} | \lambda_1 \rangle$, how much error is introduced and how do these errors affect our results?

To estimate the error in the value of $\langle \hat{\mathcal{O}} \rangle$ due to the mixedness we can define the fractional error as

$$\Delta = \frac{\langle \hat{\mathcal{O}} \rangle_p - \langle \hat{\mathcal{O}} \rangle_e}{\langle \hat{\mathcal{O}} \rangle_p} \cong (1 - \lambda_1) - \frac{\sum_{j=2}^{8} \lambda_j o_j}{o_1}, \tag{9}$$

where o_j depend on the operator involved. The experimental states have a minimum $\lambda_1 = 0.88$ while $\lambda_1 \geqslant 0.92$ in other cases. In case of all the four observables O, O_1, O_2, and O_3 we computed Δ for all the 27 experimentally prepared states and the obtained values as percentage error were in the range $1.1\% \leqslant \Delta \leqslant 9.3\%$.

In light of the errors introduced by the mixedness present in the experimentally prepared states the detection protocol has to take Δ error values into consideration in addition to the experimental errors reported in the Table III for deciding the class of three-qubit entanglement. As is evident from the above analysis, in the worst-case scenario the protocol works 90% of the time. To further increase the fidelity of the protocol, one can repeat the entire scheme on the same prepared state a number of times.

IV. CONCLUDING REMARKS

We have implemented a three-qubit entanglement detection and classification protocol on an NMR quantum information processor. The current protocol is resource efficient because it requires the measurement of only four observables to detect the entanglement of unknown three-qubit pure states, in contrast to the procedures relying on QST, where we need many more experiments. The spin ensemble was prepared in a number of three-qubit states, including standard and randomly selected states, to test the efficacy of the entanglement detection scheme. Experimental results were further verified and supported with full QST and negativity measurements. The protocol was very well able to detect the entanglement present in the seven representative states (belonging to the GHZ, W, $W\bar{W}$, biseparable and separable SLOCC inequivalent classes). A nonzero negativity indicates a genuine tripartite entanglement while a nonvanishing three-tangle implies that the state is in GHZ class, and for the randomly generated states, the protocol was able to classify the R_3, R_4, R_6, R_7, R_{10}, R_{14}, R_{16}, and R_{19} states as belonging to the GHZ class. Although the randomly generated R_{11} state has a nonzero negativity, it has a vanishing three-tangle, which implies that state belongs to the W class (which is further supported by nonzero values of the expectation values O_1, O_2, and O_3). The states R_2, R_{13}, and R_{15} were also found to belong to the W class. Vanishing expectation values for all four observables as well as vanishing negativity values indicate that the randomly generated states R_1, R_5, R_8, R_{17}, R_{18}, and R_{20} belong to the separable class, while the state R_{12} was correctly identified as belonging to the BS_3 class. We noted that, while deciding the class of an experimentally prepared state using the current protocol, one has to take into consideration the mixedness present in the actually prepared states. We estimated the errors introduced due to mixedness and found that, although the errors were nonvanishing,

their effect on the experimental classification was small, due to the high purity of all the experimentally prepared states.

With these encouraging experimental results, it would be interesting to extend the scheme to mixed states of three qubits, to a larger number of qubits, and to multipartite entanglement detection in higher-dimensional qudit systems. Results in these directions will be taken up elsewhere. Experimentally classifying entanglement in arbitrary multipartite entangled states is a challenging venture and our scheme is a step forward in this direction.

ACKNOWLEDGMENTS

All the experiments were performed on a Bruker Avance-III 600 MHz FT-NMR spectrometer at the NMR Research Facility of IISER Mohali. Arvind acknowledges funding from Department of Science and Technology-Science and Engineering Research Board (DST-SERB) New Delhi, India under Grant No. EMR/2014/000297. K.D. acknowledges funding from Department of Science and Technology-Science and Engineering Research Board (DST-SERB) New Delhi, India under Grant No. EMR/2015/000556.

[1] R. Horodecki, P. Horodecki, M. Horodecki, and K. Horodecki, Rev. Mod. Phys. **81**, 865 (2009).
[2] O. Gühne and G. Tóth, Phys. Rep. **474**, 1 (2009).
[3] M. Li, M.-J. Zhao, S.-M. Fei, and Z.-X. Wang, Front. Phys. **8**, 357 (2013).
[4] R. T. Thew, K. Nemoto, A. G. White, and W. J. Munro, Phys. Rev. A **66**, 012303 (2002).
[5] O. Gühne, P. Hyllus, D. Bruß, A. Ekert, M. Lewenstein, C. Macchiavello, and A. Sanpera, J. Mod. Opt. **50**, 1079 (2003).
[6] J. M. Arrazola, O. Gittsovich, and N. Lütkenhaus, Phys. Rev. A **85**, 062327 (2012).
[7] B. Jungnitsch, T. Moroder, and O. Gühne, Phys. Rev. Lett. **106**, 190502 (2011).
[8] A. Peres, Phys. Rev. Lett. **77**, 1413 (1996).
[9] M. Li, J. Wang, S. Shen, Z. Chen, and S.-M. Fei, Sci. Rep. **7**, 17274 (2017).
[10] D. P. DiVincenzo and A. Peres, Phys. Rev. A **55**, 4089 (1997).
[11] P. Neumann, N. Mizuochi, F. Rempp, P. Hemmer, H. Watanabe, S. Yamasaki, V. Jacques, T. Gaebel, F. Jelezko, and J. Wrachtrup, Science **320**, 1326 (2008).
[12] O. Mandel, M. Greiner, A. Widera, T. Rom, T. W. Hänsch, and I. Bloch, Nature (London) **425**, 937 (2003).
[13] M. Neeley, R. C. Bialczak, M. Lenander, E. Lucero, M. Mariantoni, A. D. O'Connell, D. Sank, H. Wang, M. Weides, J. Wenner, Y. Yin, T. Yamamoto, A. N. Cleland, and J. M. Martinis, Nature (London) **467**, 570 (2010).
[14] S. Dogra, K. Dorai, and Arvind, Phys. Rev. A **91**, 022312 (2015).
[15] W. B. Gao, P. Fallahi, E. Togan, J. Miguel-Sanchez, and A. Imamoglu, Nature (London) **491**, 426 (2012).
[16] H. Kampermann, D. Bruß, X. Peng, and D. Suter, Phys. Rev. A **81**, 040304 (2010).
[17] R. Laflamme, E. Knill, W. H. Zurek, P. Catasti, and S. Mariappan, Philos. Trans. R. Soc. A **356**, 1941 (1998).
[18] X. Peng, J. Zhang, J. Du, and D. Suter, Phys. Rev. A **81**, 042327 (2010).
[19] K. R. K. Rao and A. Kumar, Int. J. Quantum Inform. **10**, 1250039 (2012).
[20] D. Das, S. Dogra, K. Dorai, and Arvind, Phys. Rev. A **92**, 022307 (2015).
[21] T. Xin, J. S. Pedernales, E. Solano, and G.-L. Long, Phys. Rev. A **97**, 022322 (2018).
[22] M. Bourennane, M. Eibl, C. Kurtsiefer, S. Gaertner, H. Weinfurter, O. Gühne, P. Hyllus, D. Bruß, M. Lewenstein, and A. Sanpera, Phys. Rev. Lett. **92**, 087902 (2004).
[23] J. G. Filgueiras, T. O. Maciel, R. E. Auccaise, R. O. Vianna, R. S. Sarthour, and I. S. Oliveira, Quantum Inf. Process. **11**, 1883 (2012).
[24] W. K. Wootters, Quantum Info. Comput. **1**, 27 (2001).
[25] S. P. Walborn, P. H. Souto Ribeiro, L. Davidovich, F. Mintert, and A. Buchleitner, Nature (London) **440**, 1022 (2006).
[26] C. A. Sackett, D. Kielpinski, B. E. King, C. Langer, V. Meyer, C. J. Myatt, M. Rowe, Q. A. Turchette, W. M. Itano, D. J. Wineland, and C. Monroe, Nature (London) **404**, 256 (2000).
[27] W. Dür and J. I. Cirac, J. Phys. A: Math. Gen. **34**, 6837 (2001).
[28] J. B. Altepeter, E. R. Jeffrey, P. G. Kwiat, S. Tanzilli, N. Gisin, and A. Acín, Phys. Rev. Lett. **95**, 033601 (2005).
[29] C. Spengler, M. Huber, S. Brierley, T. Adaktylos, and B. C. Hiesmayr, Phys. Rev. A **86**, 022311 (2012).
[30] J. Dai, Y. L. Len, Y. S. Teo, B.-G. Englert, and L. A. Krivitsky, Phys. Rev. Lett. **113**, 170402 (2014).
[31] W. Dür, G. Vidal, and J. I. Cirac, Phys. Rev. A **62**, 062314 (2000).
[32] C. H. Bennett, S. Popescu, D. Rohrlich, J. A. Smolin, and A. V. Thapliyal, Phys. Rev. A **63**, 012307 (2000).
[33] D. P. Chi, K. Jeong, T. Kim, K. Lee, and S. Lee, Phys. Rev. A **81**, 044302 (2010).
[34] M.-J. Zhao, T.-G. Zhang, X. Li-Jost, and S.-M. Fei, Phys. Rev. A **87**, 012316 (2013).
[35] S. Adhikari, C. Datta, A. Das, and P. Agrawal, arXiv:1705.01377.
[36] A. Singh, Arvind, and K. Dorai, Phys. Rev. A **94**, 062309 (2016).
[37] A. Wong and N. Christensen, Phys. Rev. A **63**, 044301 (2001).
[38] D. Li, Quantum Inf. Process. **11**, 481 (2012).
[39] V. Coffman, J. Kundu, and W. K. Wootters, Phys. Rev. A **61**, 052306 (2000).
[40] A. Acín, D. Bruß, M. Lewenstein, and A. Sanpera, Phys. Rev. Lett. **87**, 040401 (2001).
[41] M. A. Nielsen and I. L. Chuang, *Quantum Computation and Quantum Information* (Cambridge University Press, Cambridge, UK, 2000).
[42] G. M. Leskowitz and L. J. Mueller, Phys. Rev. A **69**, 052302 (2004).
[43] R. R. Ernst, G. Bodenhausen, and A. Wokaun, *Principles of NMR in One and Two Dimensions* (Clarendon Press, Oxford, UK, 1990).
[44] D. G. Cory, M. D. Price, and T. F. Havel, Physica D **120**, 82 (1998).

[45] A. Mitra, K. Sivapriya, and A. Kumar, J. Magn. Reson. **187**, 306 (2007).
[46] A. Uhlmann, Rep. Math. Phys. **9**, 273 (1976).
[47] R. Jozsa, J. Mod. Opt. **41**, 2315 (1994).
[48] H. Singh, Arvind, and K. Dorai, Phys. Lett. A **380**, 3051 (2016).
[49] Y. S. Weinstein, Phys. Rev. A **82**, 032326 (2010).
[50] G. Vidal and R. F. Werner, Phys. Rev. A **65**, 032314 (2002).